Dicing and Grinding of Electro-Ceramics

E.L. Nix, J. Corbett, J.H. Sweet, M. Ponting
Loadpoint Ltd., Cricklade, Swindon, Wiltshire SN6 6HE, UK . Tel. +44 1793 751160
John.Sweet@Loadpoint.co.uk, J.Corbett@Cranfield.ac.uk

Abstract

There exists an ever-increasing demand for piezoelectric and electrostrictive sensors and actuators fabricated with high levels of geometrical precision and with the minimum of material damage. The applications, which include miniature high-frequency ultrasonic arrays, infrared imaging devices and printhead actuators, usually require either thin electroactive layers, or fine-pitch multi-element arrays, the former being created by grinding and lapping and the latter by dicing. This paper describes some of the techniques and equipment used for high-precision dicing and grinding at Loadpoint Ltd., the result of 30 years experience designing industrial processes for the manufacture of such devices. The focus is on the family of lead zirconate titanate (PZT) compositions, but the principles are applicable to a wide range of polycrystalline and single-crystal ferroelectric ceramics. Dicing of fine pitch and high aspect-ratio arrays is described for devices with radically different substrate configurations. An outline of the preparation of layers of piezoelectric material of thickness less than 0.1 mm with ultra-low surface roughness and practically zero damage is also presented. The influence of the material microstructure on the results achievable in dicing and grinding is discussed. The effect of the abrasion processes on the electrical and mechanical properties is also considered.

Precision Dicing

A wide range of machining operations is routinely carried out on electroceramics, including dicing, scribing, slicing, serrating, chamfering, profiling, slitting, trimming, grinding, etc. By precision dicing in particular is meant the sawing of large arrays of fingers with dimensional accuracies of the order of a few micrometers over the full device area, with low material damage and with high process yield. The tight dimensional specifications will apply in general to such quantities as finger width, finger position, array pitch, kerf depth and rectangularity.

The influence of dicing conditions, especially cutting speed, on the electro-mechanical quality of product is a key consideration. It will be seen that process yield and process throughput limits are determined by the brittle fracture properties of the individual array fingers and the relation of these properties to array geometry and microstructure. The importance of machine capabilities is outlined with reference to the NanoAce dicing platform.

Device Geometries

A wide variety of device types and configurations is encountered in practice, ranging from fine pitch arrays carried on flexible substrates, as sketched in Figure 1, to large area multilayer actuator arrays mounted on hard substrates. The electroactive medium of the device array is often combined with other materials having key functions. For example, an array may be attached to one or more acoustic layers which are important for efficient transduction of electrical to ultrasound energy. In some instances PZT arrays are in a sandwich construction, with thin polymeric acoustic layers on both faces of the PZT, the upper layer serving also to reduce array surface chipping. In contrast, an array may be bonded to a mechanically hard support layer with critical rigidity for an actuation function, such as the compression of ink in a printhead. There may also be copper track patterns or silver-epoxy fillets for electrical connectivity.

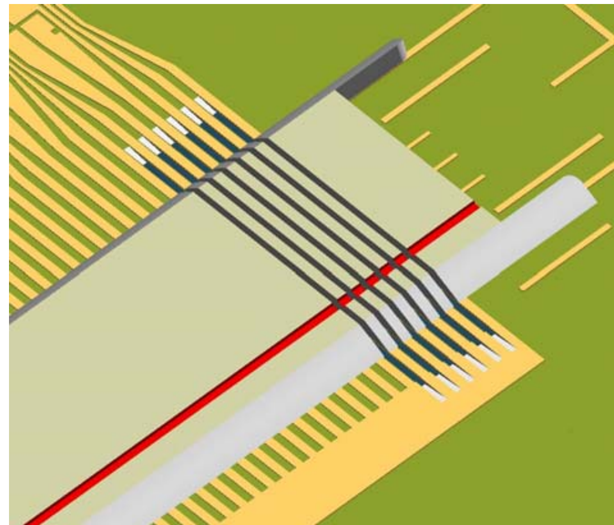

Figure 1. Dicing PZT on a Polyimide Substrate

The presence of non-ceramic materials in the device assemblies is usually a significant factor in dicing. A polymeric substrate, into which the blade must partially penetrate, may create filament streamers as the hot blade perimeter melts the polymer. Silver-palladium internal electrodes in a multilayer actuator and external silver-epoxy fillets, through which the blade must cut, may result in smearing of metal on the kerf face or in modification of blade function by clogging. A hard substrate may create excessive blade wear. Each of the device configurations and substrate types thus presents particular challenges in respect of precision dicing.

Blade Wear and Exposure

Typical saw blades are composed of 30 μm diamond grit in a carrier medium. Diamonds protruding from the bonded composite perform the abrasion. The dicing of fine pitch PZT arrays with soft substrates requires ultra-thin nickel-diamond blades with accurately balanced hubs and high-precision dressing. Electro-ceramics bonded to hard substrates usually require resin-bonded dicing blades. Many blade types are commercially available, and selection will be based on kerf-width, dicing conditions and especially on the properties of the hardest material in the device assembly. Because blades are usually selected for compatibility with hard substrates they may not be fully optimized for the piezoceramic. In such instances, blade choice is usually a compromise reflecting the composite nature of the assembly to be sawn. Blade wear for very hard substrates will necessitate intermittent height-sensing operations, especially during the dicing of large arrays. In such cases the implementation of predictive wear compensation is useful. An understanding of blade wear characteristics, and in particular the dependence of wear on cutting speed, is critical for such applications, since control of blade exposure is a factor in process stability.

Device Size and Microstructure

For high frequency ultrasound applications Loadpoint have used 11 μm nickel-diamond blades to create 64-element arrays with kerfs 14 μm wide. The array fingers were typically 27 μm wide by 48 μm deep, and operated at ~20 MHz. The array substrate material was a 25 μm layer of polyimide into which the dicing blade penetrated halfway for the purpose of acoustic channel isolation. At these tiny dimensions the mechanical quality of the piezoelectric material is in many respects more important than its electrical performance[1]. Microstructure plays a key role because the fingers are only 5 to 10 grains wide. For typical piezo-materials the mean grain size lies in the range 4 to 10 μm. Fine-grain materials (0.5 to 2 μm) are clearly relevant in miniature applications, where grain pull-outs in the kerf wall are relatively important.

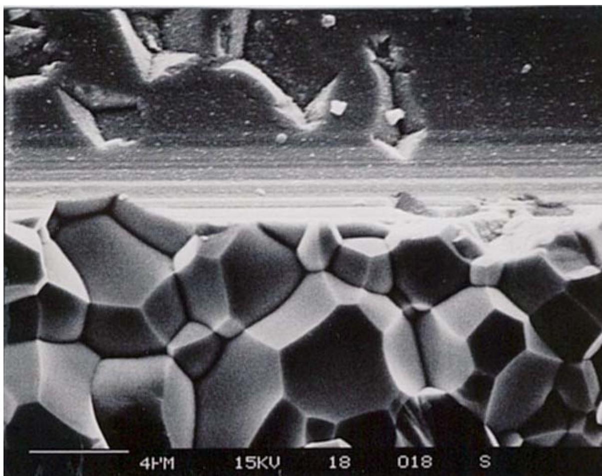

Figure 2(a). SEM of Kerf Wall and Fracture Surface

The SEM image of figure 2(a) shows the lower region of a 14 μm kerf, in which a mode 1 fracture has been initiated from the kerf base parallel to the kerf face. Individual grains of size ~6 μm are visible in the facture surface below the kerf and a number of grain pull-outs in the kerf wall can be seen. Figure 2(b) shows a lower magnification of the same kerf and fracture surface.

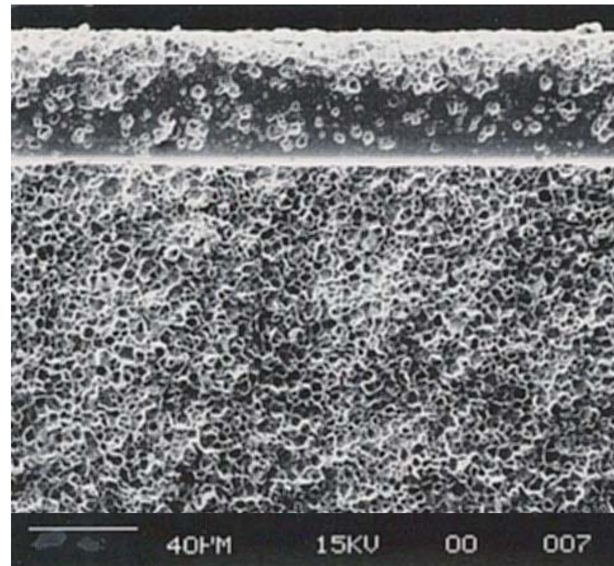

Figure 2(b). Kerf of 2(a) at Reduced Magnification

The progress of macroscopic fracture usually follows a path determined by grain boundaries. This can be seen in the kerf-wall fracture surface of Figure 2(c), where grain-boundary cracks are evident.

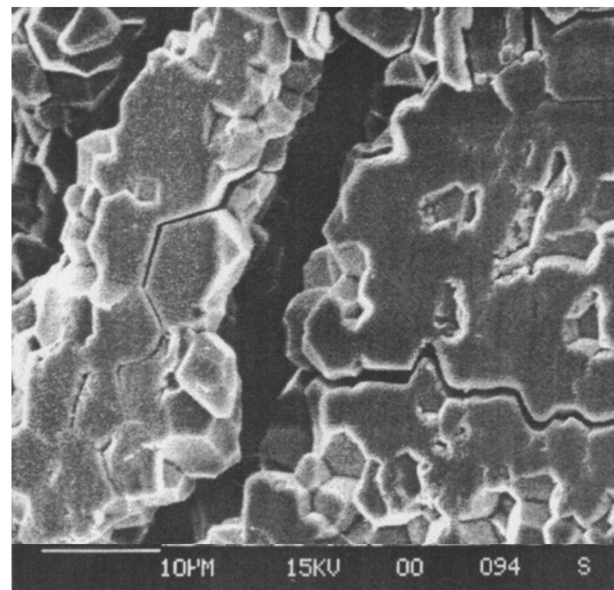

Figure 2(c). Cracks at PZT Grain Boundaries

The end use of the miniature arrays described above was intravascular imaging, where the geometry of coronary blood vessels dictates that the flexible substrates are precision-wrapped into 1 mm diameter cylinders. The final device is connected to multiplexing electronics and located at the tip of a catheter. A small

array profile is essential for access to arterial lesions. Even smaller arrays are desirable, and this trend to miniaturization is technically challenging because material microstructure and mechanical integrity have a profound impact on image quality[2]. As will be seen, the dicing process exerts stresses on an array, which can result in chipping and crumbling of individual elements.

The same mechanical considerations apply to a wide range of miniature device arrays, especially where there are unusual geometrical aspect-ratios. Thus, the sawing of arrays with tall, narrow, multilayer fingers for actuation applications requires special attention to blade choice, dressing and exposure, and to sawing speed, machine vibrations and the geometry of coolant deployment. A typical array of this kind might have a kerf depth of 800 μm and a finger width of 100 μm.

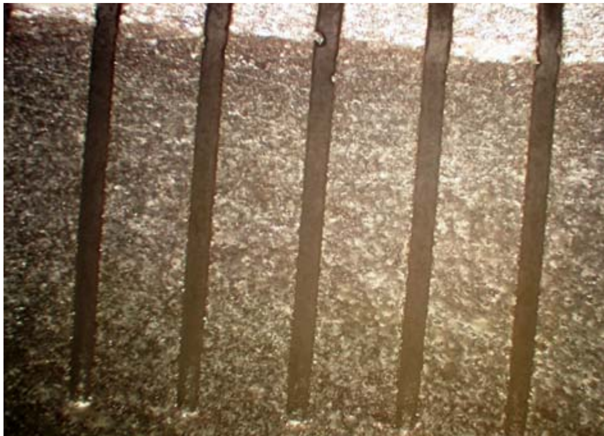

Figure 3(a). End-View of Array with Narrow Deep Kerfs

Figure 3(a) shows an image of an array diced in *Pz26*, a material supplied by Ferroperm, Denmark. The kerfs, sawn on the Nano Ace using a nickel-diamond blade, are 50 μm wide by 900 μm deep. *Pz26* is a typical 'hard' PZT with high mechanical quality factor (Q_m>1000) and low dielectric loss (tan δ~0.003). Other properties (discussed below) are d_{33}=290 pC/N, ε_r=1300 and T_C=330 °C. It is seen that deep rectangular kerfs are achievable despite that fact that SEM reveals a wide range of grain sizes (3–18 μm). However, kerf definition is enhanced with finer grain materials and fingers of width <60 μm are possible.

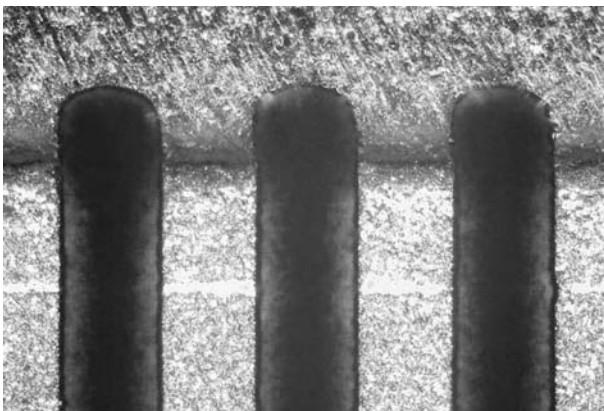

Figure 3(b). Kerf Region in a Hard Substrate Device

Figure 3(b) shows the kerf-base region of a similar high-aspect ratio array cut in a multilayer actuator mounted on a hard substrate. The substrate is shown in the upper part of photograph, and the internal electrode layers are visible in the lower part. The saw blade was resin-bonded and its wear determined largely by the substrate. The shape of the substrate kerf (here 80 μm deep) is not critical for most applications, but a reliable bond is required between fingers and substrate for high aspect ratio arrays.

Process Variables

Clearly, there exist many variables in a sawing process and close attention to a wide range of detail is critical for good dicing results at small dimensions. For the saw blade itself it is necessary to consider grit size, bonding material, blade diameter, thickness, thickness variations, flatness, hub types, exposure, balancing, dressing and wear. In respect of the cutting conditions, it is essential to take into account spindle rotation speed, spindle temperature, permitted vibration levels, cutting speed, kerf-entry speed, coolant type, lubricant type, coolant temperature, flow rate and geometry of flow deployment at the work-piece. Vibration levels are reduced by use of a high-quality air-bearing spindle and by the general rigidity of the machine construction.

Process temperatures are critical throughout. There will be an optimum temperature for the coolant and work-piece, including the vacuum mounting chuck. Control of the temperature of the environment is equally important, since thermal expansion errors are a significant factor in the sawing of large arrays to accuracies of a few μm. Cumulative errors due to thermal drift may occur, for example, during a height-sensing operation where the saw blade is away from the kerf environment for a few seconds. Machine warm-up time and stabilization are also important additional factors.

Machine Specifications

The specification of the sawing machine itself sets a final limit on the achievable results in any dicing process, and relates in particular to the quality of the lead screws, linear and rotary encoders and general machine geometry. For the Loadpoint Nano Ace, shown in figure 4, the positional resolution of the dicing platform is ±0.1 μm on the y and z axes, ±0.2 μm on the x axis and 0.0001 degrees on the θ axis. The absolute positioning is ±1 μm on x, y and z axes. There is a high axial acceleration capability which reduces the time required for non-cutting movements. This increases process throughput, but inertial forces must be maintained at acceptable levels to minimize unwanted vibrations and distortions. Finally it may be remarked that high resolution metrology is required to examine the results of a precision dicing process. In general the kerf measurements also require some degree of automation if adequate statistical data is to be collected for characterization of large arrays. A full understanding of process output characteristics is required for control and optimization.

Figure 4. NanoAce Dicing Machine

Selection of Materials

The following discussion is of a general nature, its purpose being to highlight the multi-variable nature of the choice of material properties for electroactive devices. Compositional information from PZT suppliers is usually incomplete for commercial reasons, but it is evident that a wide range of material modifications is available, and that mechanical, electrical and optical properties can be tailored to meet various needs[3-5]. Doping elements include niobium, lanthanum, magnesium, zinc, nickel, uranium and others, but common to most compositions are lead, zirconium and titanium oxides from which the family abbreviation PZT is formed.

Applications with composite structure require specific combinations of materials properties. In many cases the PZT properties cannot be optimized without reference to the whole structure. Materials selection may thus be a compromise between requirements which conflict, and must take into account the presence of all the components which comprise the assembly. In particular the temperatures encountered in the device processing route may reduce piezoelectric response. As already mentioned, miniature array applications require PZT formulations optimized with special reference to mechanical integrity. Intravascular ultrasound arrays additionally require materials with high permittivity[2] (e.g. $\varepsilon_r \sim 5000$), since the transducer is positioned at the end of a long transmission line (the catheter). For efficient transduction some devices will require high values of both thickness-mode piezoelectric strain coefficient d_{33} and mechanical coupling factor k_{33}. Additionally, for production-processing of devices at elevated temperatures, such as may be required for adhesive bonding, a high Curie temperature, T_C, is desirable. Since the dicing process itself generates local heating in the kerf, thermal degradation is often a consideration. However, the high T_C may conflict with the requirement for high d_{33}. Strongly piezoelectric PZT materials usually have lower T_C values and are therefore more prone to depolarization during dicing and other processing steps. Thus, Ferroperm *Pz26*, with its modest d_{33} response of 290 pC/N, has a high T_C of 330°C. In contrast, a highly active material, such as Advanced Ceramics Ltd *4055HP*, with reported d_{33} value 800 pC/N, has T_C as low as 145°C. For very large area arrays, uniformity of response may be a further property of importance. In multilayer actuators with several internal electrodes, some non-uniformity arises from differential shrinkage during sintering. It is difficult to measure d_{33} accurately and therefore non-uniformity of this kind is not easy to assess[6].

Fine Grain PZT

Fine grain PZT materials[7-9] are of interest in precision dicing because they offer high uniformity, high Weibull modulus and enhanced values of fracture strain. Weibull modulus, m, is a useful characterization parameter for polycrystalline ceramics[10]. Materials with low m have less predictable fracture strength and the design safety margin must be correspondingly greater. Thus, the value of m, which typically varies from 8 to 25 for sintered PZT compositions[11], is as important as the conventional strength in the discussion of fracture. A low value of m is usually associated with an increased concentration of intrinsic flaws. The poor mechanical performance of some PZT materials in dicing has been linked with low Weibull modulus. These PZTs are also found to be difficult to grind and lap to very thin sections[1].

In general fine-grain materials show the enhanced mechanical properties associated with high Weibull modulus. The downside is the modest electrical properties often associated with reduced grain size. The 200 FG grade available from TRS Ceramics, for which the grain size is said to be 0.5 µm, is a typical example of this problem. The Weibull modulus (22.4) and fracture strain (0.34%) compare favourably with other PZT materials, but the thickness-mode piezoelectric strain response (d_{33}=350 pC/N), permittivity (ε_r=1810) and coupling coefficient (k_{33}=68%) may be regarded as too low for some applications. In contrast, the C3900P grade from Aura Ceramics, for which the mean grain size is of the order of 6 µm, has useful electrical properties (d_{33}=750 pC/N, ε_r=3900, k_{33}=78%) but mediocre Weibull modulus and fracture strain (10.2 and 0.19% respectively). Materials data of this type is usually supported by the dicing and lapping results, which are inferior for the low Weibull modulus materials. However studies have not shown a clear correlation between the inherent flaw size and the material grain size seen in SEM examinations.

Single Crystals

Single crystal materials are currently rather expensive for devices intended for low-cost, high volume markets, but they can offer astonishing properties. An example of this group of materials is lead-zinc-niobate (abbreviated to PZN). A flux-grown PZN of composition PZN-8%PT is reported[12] to have d_{33}~2200 pC/N, k_{33}~94%, ε_r=5690 and T_C~185°C. It is noteworthy that the fracture strain varies significantly amongst sintered PZT materials and may be in the range 0.18 to 0.34%. In contrast, the fracture strain of single crystal PZN is said to be 1.5%, which makes this material very tough in practical applications. Fracture data is not generally available for single crystal materials because of the high cost of procuring samples. However, extensive piezoelectric and mechanical data has been presented[12,13].

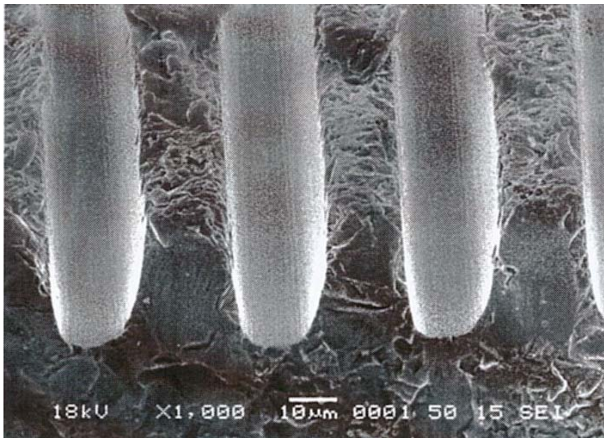

Figure 5. Kerfs 15μm x 50μm in Single Crystal PZN

Preliminary fine-pitch dicing of 0.6 mm thick samples of single crystal PZN-8%PT shows excellent kerf-wall properties under SEM examination, as seen in figure 5. If the cost of such materials can be reduced to commercially acceptable levels, especially with reference to disposable devices, then single crystals will become important for a wide range of applications because of their exceptional electromechanical properties.

The Dicing Process

The finger sawing process is essentially abrasive. The abrasion creates both compressive and tangential forces in the kerf, the former dominating. As would be anticipated, the abrasion aggravates existing cracks and also creates new ones. The new cracks are mostly vertical beneath the saw blade, because the diamond grit particles of the blade composite produce a vertical indentation force. In multi-layer devices with internal electrodes, cracks underneath the saw blade that are initially vertical are drawn to electrode layers beneath and veer away parallel to the interface as a result of the intrinsic asymmetry of the sawing process. This asymmetry arises because there is continuous ceramic on one side of the dicing wheel and a set of narrow fingers on the other side. Sideways forces in the kerf, generated by blade, debris and coolant, create a cantilever deformation which can be significant for tall, narrow fingers. Thus, fracture tends to occur at internal electrodes in tensile mode 1. As would be expected, the fracture energy of the interface surface, representing the degree of adhesion, is a key parameter, as also is finger width. The electrode-interface fracture energy is typically much smaller than the fracture energy of the bulk electro-ceramic.

It is instructive to consider the origin of forces in the kerf and the mechanisms by which heat is generated and dissipated. The dicing blade fills the kerf except for a thin layer of coolant and debris, which undergoes rapid shear. Considering the limited case of pure water undergoing Newtonian shear, it is a straightforward matter to show that the rate of heat generation W is proportional to the area, A, of blade adjacent to the kerf wall, the square of the blade diameter, D, and the square of the rotation speed, f. Similarly it is found that the drag force on the blade, F, is directly proportional to the product ADf. Typically, for coolant shear alone, F is a few tenths of one Newton and W several tens of watts. Clearly, power is also required to demolish the electro-ceramic and move the debris through the kerf. This generates further local heating and additional force, but is more difficult to assess. The instantaneous local temperatures can be sufficiently high for PZT depolarization. A hot zone is sometimes visible on the advancing perimeter of the blade. If an array is starved of coolant for a few seconds during dicing, burn marks in the kerf appear accompanied by delamination of interface layers. An experimental study is underway, designed to estimate the power dissipated by means of changes in the spindle electrical drive parameters. For some devices, an understanding of kerf hydrodynamics may prove fruitful for dicing process improvements. The geometry of the coolant supply to the blade and kerf can also have a significant effect on the dicing process. This is probably associated with access of coolant to localized hot zones. Optimum configurations are usually found by empirical methods.

The thermal asymmetry of the dicing process thus gives rise to small differences in the electrical properties between the two faces of a diced finger, an effect which increases with array density. On one side of the kerf heat is conducted to a single finger but on the other to continuous undiced ceramic. The main heat transfer is, of course, to the coolant and substrate. Whilst transient thermal phenomena are short-lived on the sub-millimetre scale, they are of more significant duration at larger dimensions. A measure of the duration of thermal transients is given by $\tau=\ell^2/\alpha$ where ℓ is the dimension in the direction of heat flow and α is the thermal diffusivity. If the finger width is 80 μm and $\alpha=1.5\times10^{-6} m^2 s^{-1}$ (for a typical piezo-ceramic array) then $\tau<5$ ms. In contrast, for the uncut ceramic where ℓ is of the order of mm, τ is of the order of seconds. It is conjectured that the uncut material experiences the elevated temperature for a longer period and undergoes more depolarization. Estimation of dicing damage, both thermal and mechanical, is discussed further below.

Fracture Mechanics

Ceramic materials, such as PZT and alumina, fail by brittle fracture without measurable plastic deformation. In general, failure is controlled by pre-existing flaws, such as grain-boundaries, pores, cracks and inclusions, but these defects are hard to detect except by destructive tests. Typical electro-ceramics contain a distribution of inhomogeneities, the distribution varying between different chemical compositions and for modifications of the processing of chemically identical compositions[14]. Multi-layered actuator composites may also exhibit defects at internal electrode layers.

For both electrical and mechanical applications, the properties of sintered ceramics reach their optimum values at the highest densities. Therefore attainment of the best results usually means the elimination of porosity by isostatic or uniaxial hot-pressing, either in a high pressure gas or in an inert ceramic medium. For tape-cast multilayer actuators optimum sintering conditions may not be possible, and therefore the mechanical properties may not reflect the best achievable in the equivalent bulk material. Additionally, piezoelectric media exhibit fracture properties which are different from their non-piezoelectric counterparts[15-18].

A small crack or discontinuity in a ferroelectric ceramic, which might reside at a domain wall or an interface layer, gives rise to stress intensification at its tip region[19]. The intensified stress initiates crack growth and macroscopic failure. The initial discontinuity may be an intrinsic feature of the ceramic microstructure, such as a weak grain boundary, or an extrinsic feature resulting from surface grinding or dicing. If the embryonic discontinuity is not a crack, then a crack develops prior to failure. Spontaneous propagation occurs when the Griffith instability criterion[20] is met, that is, when the stress reaches the critical value given by $\sigma_C=\sqrt{YG_C/\pi a}$, where Y is the elastic modulus, G_C is the fracture surface energy and a is the crack half-length in an infinite plate. It is seen that failure stress can vary widely without the fundamental material properties Y or G_C changing at all. In general, high strength materials have low fracture toughness, and fracture can be discussed in terms of the concepts of linear elastic fracture mechanics. These concepts are based on elastic plane-strain solutions which are applicable when the crack tip plastic zone is small compared with the length of the crack itself. The variation in strength between different samples of the same chemical composition depends on the range of flaw sizes, which is related to processing and other features not necessarily connected with composition.

As already mentioned, strength is best characterized by a Weibull analysis, which takes into account the statistical nature of the distribution of flaws. Clearly, it is of practical value to be able to estimate the mean size of intrinsic flaws, and experimental techniques based on the measurement of macroscopic properties are available. These methods involve the creation of artificial cracks of known size, and the determination of the fracture toughness.

Finger Fracture

The goal of fracture mechanics, as applied to the dicing of electro-ceramics, is to model finger fracture as a function of material properties, cut depth and finger width, assuming the theory of linear elastic fracture mechanics. A model of fracture must assume a fracture mechanism, such as already outlined for multi-layered devices. To test the validity of the model, measurements of cutting force are required, in particular the dicing load as a function of material and process variables. Determinations of the critical stress intensity factors, K_C, for the bulk piezoceramic and the intermediate electrode layers are also needed. Conventionally these tests use the standardized compact-tension method (ASTM E399). Supporting data may be provided by the determination of the lateral finger fracture force, either by means of a narrow-wedge forced into the kerf until fracture, or by the use of a micro-cantilever fracture test. The wedge-test has the merit of simplicity and can be used to evaluate the quality of the sawn product. The more refined cantilever test is suitable for statistical analysis, and studies of this type are in progress.

Modeling calculations are usually based on a two-dimensional finite-element approach and the results give strain-energy release rate, G, as a function of crack-length, *a*. A basic premise is that the energy released when the crack-length changes determines whether cracking occurs. Crack growth will occur when G is greater than the critical value G_C, and the growth will be unstable when $\partial G/\partial a>0$. For monolithic materials in plane-strain, G_C and K_C are related through the elastic modulus, Y, and Poisson ratio, ν, by $G_C=(1-\nu^2)K_C^2/Y$. More complicated relations hold for interfaces. For multi-layered actuator arrays, the primary interest is the strain-energy release rate for cracks parallel to the electrode interface, since this relates closely to finger fracture in the device. The interface fracture energy is typically smaller than the bulk fracture energy, and in some cases less than half.

Stable Cracks

A key analytical result is that parallel cracks less than a certain size are stable, for given kerf geometry and material properties. A further result is that the kerf depth has much less effect on crack stability than does the finger width. However, in this case it is likely that lateral pressure from coolant, kerf debris and wheel vibrations (which are not fully accounted for in the analysis) will create some dependence on depth of cut. The maximum size of stable cracks diminishes sharply with decreasing finger width and this has profound implications for manufacture, since process yield is wholly dependent on the stability of intrinsic flaws. Clearly, from the perspective of the manufacture of large arrays of fingers, process yield considerations are paramount. For given finger width, in a manufacturable device, the maximum size of stable cracks must be greater than the intrinsic flaw size. In this case there is, in principle, an assurance of process stability. However,

it is the width of the distribution of cracks, as much as the mean size, which defines the manufacturing process window. Yield is related to defect distribution. A small fraction of defects, whether pre-existing or created by the saw blade, may be outside of the stable range and thus reduce manufacturing yield. Since a single broken finger may render a whole device array unusable, the empirical determination of fracture statistics for interface layers is important in forecasting process yield. The intrinsic crack length is sometimes assumed to be of the order of magnitude of the grain size, and so typically about 5 µm. However, there is no experimental evidence to substantiate a direct connection between grain size and intrinsic flaw size, and it likely that there are larger defects present in a normal PZT ceramic.

Actuation Fatigue

The reduction of processing cracks is also important from the point of view of product lifetime. Once a crack exists in a piezoelectric medium, actuation forces may create crack-driving forces which finally create failure by fatigue[21]. Both load-cycling and the expansion and contraction of temperature-cycling[22] will be contributory factors in crack growth. It is difficult to quantify the significance of cracks for product lifetime, and determinations are usually empirical. In general the physics of fatigue fracture is not well-understood for electro-active materials, although there is much recent literature, including studies of the fatigue behaviour of actuators[23-29].

Cutting Force

It is noteworthy that the dicing ‘pressure’ in the kerf is exerted only on the small percentage of cutting diamonds which protrude and perform the abrasion. The surface fraction of diamonds is not precisely known but is typically less than 10%. SEM can be used to provide an approximate value. For a given set of material properties (such as interface fracture energy, bulk fracture toughness, grain size, intrinsic flaw size) the vertical cutting force, F, is the key factor in finger fracture. The exploration of those dicing parameters which can reduce the sawing force is therefore a critical pursuit.

Cutting force is related directly to cutting speed. It also varies with longitudinal position in the kerf, reflecting the changing blade-kerf contact area and the device composite structure (substrate, etc). Tangential forces in the kerf are known to be small and are dominated by the vertical cutting force. The influence of cutting speed can be seen from the increase of spindle-current with machine feed rate. Although most of the spindle load results from shearing coolant and debris in the kerf, it is typically possible to discern a linear increase of spindle-current with feed rate until a critical value is reached. At this critical speed there is no further increase in power delivered to the spindle, but device damage accelerates rapidly. The final choice of cutting speed is therefore inevitably a compromise between desired process throughput and acceptable process yield.

Under given cutting conditions (e.g. blade type, speed, temperature) the cutting force appears to be closely linked to material properties. There is evidence that a smaller grain size leads to a smaller cutting force, and indications also of a direct correlation between cutting force and bulk fracture toughness. Grain or domain hardness may also play a role which could be determined by indentation techniques[30].

Empirical studies have indicated that the cutting force at the critical finger width varies approximately as g to the power ⅔ where g is the size of the largest grains. If this result is of general validity then it may be concluded that a narrow distribution of grain sizes, as well as a small mean size, promotes a reduction in cutting force. This is approximately in line with experience of fine grain materials. It is proposed that the saw force is caused by the fracture toughness of the bulk piezoceramic material. Thus F is directly proportional to K_C and therefore proportional to $\sqrt{G_{CB}}$ where G_{CB} is the critical value of the stored energy for crack growth in the bulk PZT.

For multi-layered devices with internal electrodes, analytical studies show that the critical finger width at fracture is proportional to $F/\sqrt{G_{CI}}$, where G_{CI} is the critical surface energy of the interface layer. Combining this with the above result for grain size, it is seen that the conditions for the achievement of narrow fingers in multilayer actuators are: (i) small grains; (ii) a narrow distribution of grain sizes; (iii) low fracture toughness of the bulk piezoceramic; and (iv) high fracture toughness of the interface electrode layer. Fracture toughness varies widely between different PZT compositions[31-33], typically ranging from 0.3 to 1.2 MPa√m. Smaller grains appear to promote higher fracture toughness, but the correlation is not strong. K_C for internal electrode layers is always smaller than the bulk value.

For very fine pitch arrays, in which finger widths are so small that only a few grains are present over the width of a finger, the validity of continuum models of fracture is questionable. The same caution applies to continuum models of electrode interface layers, where an intermediate co-fired metallic layer may contain discontinuities. Nevertheless, it is a fact of experience that fingers with fine grain structure survive to narrower widths in reducing finger-width experiments, in line with continuum models.

Dead Zone Estimation

In addition to propagating existing cracks and initiating new ones, the dicing process also creates piezoelectric ‘dead zones’ a few micrometres thick adjacent to the kerf which reduce the activity of the array fingers. Strictly speaking the zones are not entirely inactive, but consist of piezoceramic which is both mechanically and thermally damaged. Loss of activity is caused by local heating in the kerf, poor wall definition, grain pull-out, cracks and other factors. For fine pitch arrays, with fingers only 30 to 80 µm wide, the damaged zones can have a relatively large impact on the array performance.

Successful models of the damaged zones have been proposed which are broadly supported by electrical measurements. Typically these models suggest a 2-4 µm layer of mechanically damaged material directly adjacent to the kerf, connected to a second thermally damaged layer 6-8 µm thick. It is proposed that the first layer has a much reduced dielectric constant resulting from cracks and other surface layer discontinuities. The activity of this mechanically damaged layer cannot be recovered. The second layer has a reduced polarization resulting from thermal transients during the dicing abrasion, and a dielectric constant reduced by typically 20%. The thermal depolarization is largely recoverable by the application of an electric field, either as part of the manufacturing process, or subsequently in service.

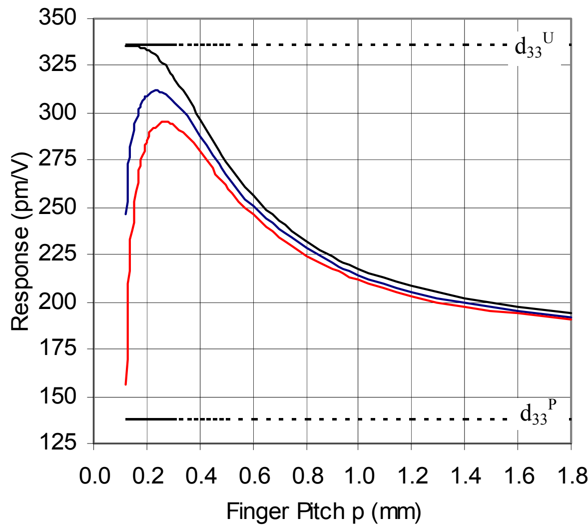

Figure 6. Effect of Constraints and Dead Zones

The difficulties of assessing the dicing damage are exacerbated by changes in the electrical response of the array arising purely from the changing mechanical constraints introduced by dicing. These changes can arise from release of internal stresses in the piezoelectric medium itself (such as exist in a multilayered actuator with internal electrodes) or from the change from planar to uniaxial constraint for a piezoelectric layer bonded to a rigid substrate.

For example, the d_{33} coefficient in full planar constraint is reduced to typically 35% of the free value. The planar value is given by $d_{33}^P=e_{33}/c_{33}$ where e_{33} is the piezoelectric stress coefficient and c_{33} is the elastic stiffness. On dicing to very narrow fingers the planar constraint is changed to a unidirectional constraint, and the response increases to $d_{33}^U=d_{33}+v_{31}d_{31}$, where v_{31} is Poisson's ratio and d_{31} is the lateral piezoelectric strain coefficient. Typically d_{33}^U is 75% of the free value. This is illustrated in figure 6 where the d_{33} response is shown as a function of finger pitch. The upper and lower dotted lines are the limiting values d_{33}^U and d_{33}^P respectively for a typical PZT material with d_{33}=400 pC/N. The curves shown are for fully inactive zones of thickness 0, 4 and 8 µm. The diminishing response of the more dense arrays arises from the proportionately larger effects of dicing-damage at fine pitch.

Similar changes occur in the dielectric constant κ, which has the significant advantage of being more amenable to direct measurement. Here $\kappa^P=\kappa+2d_{31}^2c_{31}/(s_{31}c_{33})$ where κ^P and κ are the planar and free values respectively, c_{33} and c_{31} are normal and lateral stiffnesses, and s_{31} is a lateral compliance. Typically the planar constrained value is 65% of the free value. On dicing κ increases from the planar to the uniaxially-constrained value given by $\kappa^U=\kappa-Y_1d_{31}^2$, where Y_1 is the elastic modulus along the finger length. κ^U is typically 85% of the free value. A plot of dielectric constant versus finger pitch has a shape similar to that of figure 6. The effect of thermal damage on the value of κ can be measured using a fully depolarized bulk sample. The effect of mechanical damage is more difficult to estimate; a layer of material with zero dielectric constant is a rough approximation. In general it is seen that the effects of the mechanical constraints can be calculated, and the effective dicing damage estimated, only when the piezoelastic anisotropy[34] and the constraining influence of substrate layers are both fully understood.

If the piezoelectric medium and substrate have matched thermal expansion coefficients then an unconstrained pyroelectric assessment of dicing damage is an option. If the pyroelectric response of the whole array is measured before and after dicing, and the ratio of diced and undiced instantaneous pyroelectric currents, i_D/i_U, is plotted as a function of kerf fraction Nk (where N is the number of kerfs per unit length and k is the kerf width), then the gradient of the plot is $-(k+2\delta)/k$ where δ is the dead zone width. Alternatively, at given dicing pitch, p, the total dead width per finger is given by $2\delta=p(1-i_D/i_U)-k$.

It is not usually desirable to have to re-polarize whole device arrays or individual channels which have been partially de-poled by adverse dicing conditions. Activity reduction may be acceptable if it is uniform across an array. The choice of dicing temperature, coolant, blade type, rotation speed and feed rate will all influence the damage done the PZT and in this respect the selection of Curie temperature is important. A high T_C is desirable if depolarization is to be reduced to low levels, but an alternative approach is to select a material with a low T_C and repolarize by means of a permanent bias field in service use of the device. With a high T_C material some recovery of depolarized fingers is possible, but it may be incomplete or slow.

Further Studies

The foregoing general discussion has indicated the complicated interrelationship of material microstructure, electromechanical properties and process variables in the dicing of arrays of fingers in electroceramics. Clearly, there is wide scope for fundamental studies and these are encouraged in the expectation that they will generate further understanding of the physics of dicing and point to process improvements and high yield manufacturing routes for the miniature devices demanded by the instrumentation markets.

Precision Grinding

The last twenty years has witnessed an increased activity in the development of ultra-precision grinding machines designed to meet the increasing demands for reduced dimensional tolerances together with high surface and sub-surface integrity on advanced 'difficult- to-machine' materials. Amongst the most difficult materials to machine are those that are hard and brittle, such as glasses or engineering and functional ceramics. However, machining remains an important process for the manufacture of devices for a range of industries, including semiconductor, optical communication, computer-peripheral, medical and aerospace. To take one example, piezoelectric bimorphs are widely used as mechanical drivers, sound generating or receiving devices and general purpose displacement actuators. Bimorphs are usually constructed by adhesively bonding layers of a piezoelectric ceramic onto an elastic plate. Applying an electric field to the piezoelectric layer induces a strain which is asymmetric about the bond line, causing the whole structure to deform in bending. The structural integrity of the bond line is thus critical to the mechanical performance and reliability of the device. High surface quality, in terms of flatness and roughness, is desirable for the ceramic components as it enables a very thin and hence structurally efficient bond to be made[35]. To address this kind of problem, and a wide range of similar industrial needs, the second part of this paper is devoted to surface integrity control during the precision grinding of brittle materials, with particular reference to PZT.

Damage-Free Machining

Machining processes for brittle materials are dominated by diamond turning and diamond grinding. A key requirement is the ability to control surface integrity during machining processes whilst maximizing material removal rates and minimizing production cost. Important surface integrity issues include surface finish, residual stress and localized microfracture-microstructure effects. This has placed arduous requirements on both the machine tools and the associated tooling. Higher precision machine tools have been developed and tool preparation methods have been improved.

The material removal process can be considered broadly in terms of fracture dominated mechanisms or localized plastic deformation. For conventional machining of brittle materials, fracture processes result in localized surface damage that may compromise material properties and performance. For many applications this surface damage must be removed by lapping and polishing processes which tend to be time consuming and expensive whilst also possibly compromising form accuracy. To address this problem much effort has been put into the development of 'damage free' or 'ductile regime' machining[36]. The concept of 'ductile regime' grinding assumes that localized plastic deformation can occur in brittle materials within a small controlled volume in the machining zone.

Material Properties

Plastic deformation of the machined material becomes energetically favourable as the scale of deformation decreases, and hence there is a volume below which material will deform plastically and not fracture. This has led to the development of theoretical models which predict the 'critical depth of cut', which is assumed to be a function of the deformed volume, that results in brittle fracture.

The ability to predict optimum machining conditions and the safe envelope of operating parameters is essential if effective machining processes are to be developed. To predict 'ductile regime' machining conditions considerable effort has been focused on relating the on-set of surface and sub-surface damage during machining to quasi-static indentation. An indentation fracture mechanics approach can be used to predict the on-set of fracture based on small scale indentation events to simulate tool/abrasive – workpiece interactions. Deformation/fracture diagrams normalized with respect to hardness and fracture toughness[36] are useful in identifying the critical load for the on-set of fracture. Below this critical load the tool/workpiece interaction is deformation controlled and no fracture damage is observed. The concept of a critical load can be extended to chip thickness. As the chip thickness increases the load should also increase for a given contact situation. It should therefore be possible to relate a critical load for the on-set of fracture to a critical chip thickness or equivalent depth of penetration[37].

The transition loads from 'ductile' to 'brittle' machining for softer ceramics, such as PZT materials (Hv~300 kg/mm^2), are more difficult to identify as the boundary between ductile and brittle behaviour is more diffuse and also depends on local variations in material microstructure and composition. The cutting forces may be high enough to modify the workpiece material characteristics. In PZT this can be in the form of textural changes which modify the material ferroelectric properties. X-ray diffraction techniques can be used to assess such textural effects and methods using synchrotron radiation have proved useful in determining the depth of 'damage'.

Grinding Processes

Certain ceramics are more difficult to grind depending on their composition and mechanical properties. PZT is an example where grain pull-out and wheel loading can cause major problems. Figure 7 illustrates a PZT surface ground with a 3–6 µm diamond resin bond wheel, using a 0.1 mm/s feed rate, wheel speed of 30 m/s and depth of cut of 0.5 µm. A poor surface results[38] exhibiting much grain pull-out and a surface finish of around 250 nm Ra. Even though the grinding parameters were chosen to give a small chip thickness, the grinding forces soon increased due to the poor cutting efficiency of the abrasive and loading of the grinding wheel with PZT.

The problem identified in figure 7 is an example which highlights the dynamic characteristics of the grinding process[37]. Care is taken to true and dress grinding wheels to ensure optimum cutting conditions but the abrasive-workpiece contact conditions continually change due to grit wear, a change in the number of active grits and wheel loading problems. To optimize the grinding process efficiency it is essential to maintain an optimum wheel condition. This can be best achieved through wheel dressing technology.

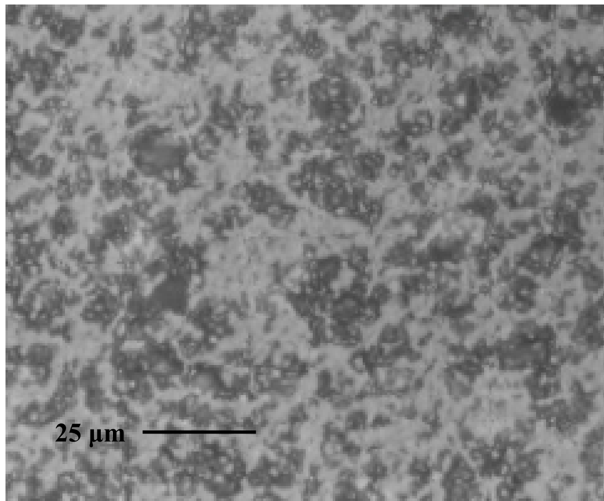

Figure 7. PZT ground surface illustrating grain pull-out and poor finish[38]

An important development in dressing technology which has proved suitable for fine grit grinding wheels is that of electrolytic in-process dressing (ELID)[39]. This technique, developed by Nakagawa and Ohmori[39,40] was an extension of earlier research carried out by Buttner[41]. The ELID technique ensures that an adequate grain exposure is maintained during grinding. One of the potential benefits of ELID is the ability to minimize the individual grinding grit cutting force, thereby making higher material removal rates possible. These benefits can be extended to the grinding of more difficult materials such as PZT.

The surface appearance of PZT, machined with conventional resin bond and ELID metal bond ground surfaces, is shown[38] in figure 8. Using ELID, a surface finish of around 5 nm Ra can be achieved and the only major defects relate to residual porosity within the original ceramic. Force measurements during grinding show that the force per grit is reduced by more than an order of magnitude when grinding PZT with ELID and this accounts for the much improved surface quality and absence of grain pull-out. A further benefit of the low grinding forces is the much reduced depth of damage due to textural effects. X-ray diffraction measurements demonstrated that this type of damage extended only 2 µm into the material compared with 6 µm for resin ground surfaces and 11 µm for diamond turned surfaces[38].

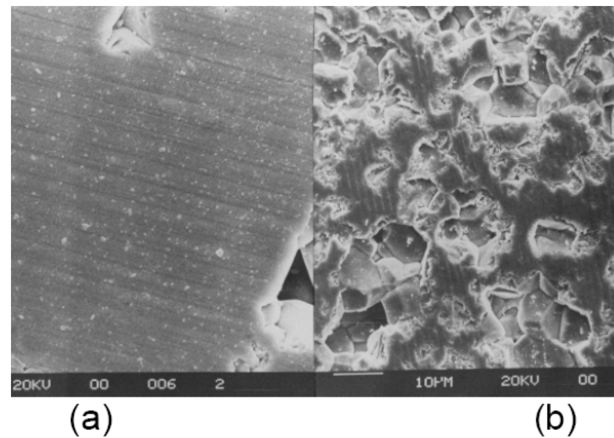

Figure 8. Surface appearance of diamond ground PZT: (a) ELID; (b) no ELID (4)

Figure 9 shows an example of how precision grinding processes can be integrated with micro-fabrication techniques[37]. The photograph shows, from the base up, a 100 mm diameter, 400 µm thick silicon wafer bonded to a 50 mm diameter, 50 µm thick PZT wafer, 12 µm of titanium and a second 50 µm thick PZT wafer with associated electrodes.

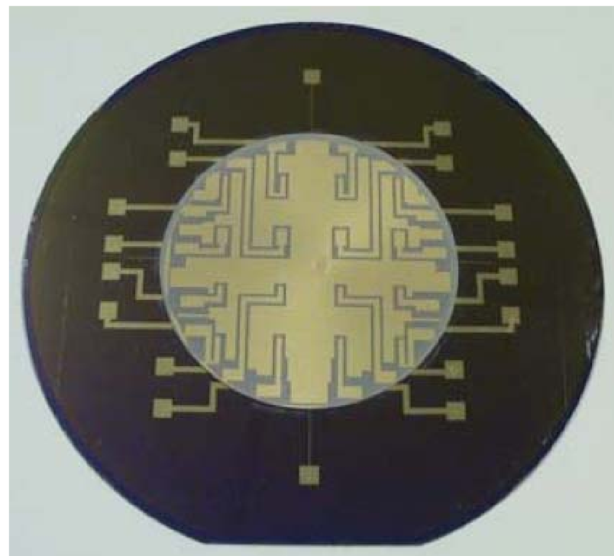

Figure 9. MEMS-based boundary layer flow separation control system, in collaboration with BAE Systems Advanced Technology Centre, Sowerby, UK

The major challenges associated with the manufacture of this device have been to ensure damage free grinding of the silicon and PZT wafers and the attainment of the necessary parallelism. The overall flatness for the PZT layers is ±1 µm, whilst surface finish is only required to be 20-30 nm Ra, which is still good compared to most commercial ceramics. Achieving sub-100 µm thick layers of PZT of this quality is not feasible by other means. The alternative method of lapping and polishing is very slow and expensive, whilst thick film deposition techniques do not produce material that has the necessary electro-active properties.

Ultra-Precision Grinding Machines

The design of ultra-precision machines is fundamental in improving machining performance by, for example, designing for high dynamic loop stiffness, the minimization of thermal effects and friction and the incorporation of advanced measurement and control systems. For a number of years Loadpoint Ltd and Cranfield University have worked together to develop machine tools with the attributes listed above, which result in the precise control of the abrasive-grit and workpiece interaction during grinding, such that the chip thickness can be maintained below critical values whilst maximizing the stock removal rate and minimizing surface roughness. The work evolved via the initial development of Tetraform 'C'.

The Tetraform(™) concept originated from a machine tool design by Lindsey at the UK National Physical Laboratory[42]. Tetraform 'C', designed and built by Loadpoint, comprises a pin-pointed tetrahedral structure shown in figure 10. Three struts of equal length are joined with 'fixed' ball-ended joints to form a horizontal base. The other three struts are joined with similar joints and they support a connecting unit that also houses the machine spindle and 'Z' vertical slide-way. The horizontal 'X' and 'Y' slide-ways are attached to the base struts and their maximum strokes are 220 mm and 120 mm respectively.

Figure 10. Tetraform 'C'

The 'Z' axis travel is limited to a maximum of 20 mm. The machine is currently provided with three aerostatic spindles. A vertical grinding cup wheel spindle, with an integral drive motor, is fitted to the 'Z' slide-way, although this may be replaced with a horizontal spindle intended for slitting or dicing. This horizontal spindle is a standard Loadpoint LDS 7 dicing spindle with an integral brush-less DC drive motor. The third aerostatic spindle is a 'stiff' truing/dressing spindle.

An example of the 'ductile' regime grinding of glass is shown in figure 11 which illustrates an atomic force microscopy (AFM) image of ground quartz. This surface was produced using a metal bond diamond wheel (3–6 µm grit size), 10 µm depth of cut and 6 mm/min feed rate to generate a surface of 1.4 nm Ra. A second pass of 1 µm depth of cut at 1 mm/min reduced the Ra to 0.6 nm as measured on the AFM.

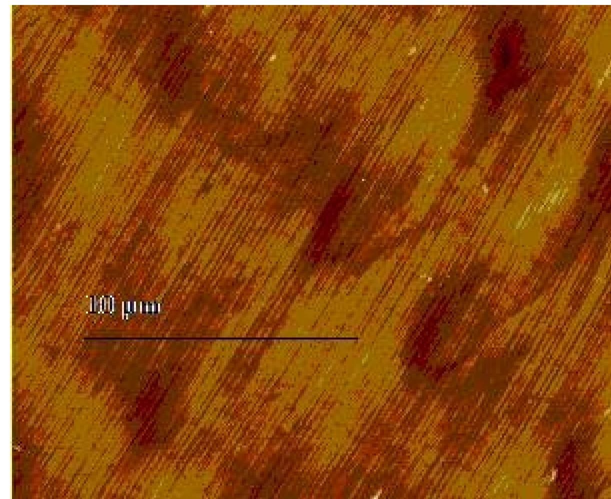

Figure 11. AFM image of ground glass surface.
Surface finish measured at 0.6 nm Ra

Grinding of silicon wafer material on Tetraform 'C' was undertaken using a resin bond diamond cup-wheel with a 3–6 µm grit size. A wheel speed of 6000 rpm (39 m/s), feed rates up to 10 mm/min and depths of cut up to 10 µm were used. The results showed that precision ground surfaces could easily be produced. For example, a test piece was ground with Ra=2.17 nm, at a worktable speed of 6 mm/min and using a depth of cut of 8 µm. The Ra value compares favourably with the as-polished finish that is typically between 1 and 2 nm Ra.

In the year 2000 Loadpoint commenced development of an improved machine tool incorporating the high static and dynamic stiffness of the Tetraform 'C'. The machine, PicoAce™, provides accessibility for automated work handling, together with sufficiently long axes for semiconductor-industry-standard 300 mm diameter materials processing. The first production model of PicoAce, shown in figure 12, was installed at Loadpoint's facility in Swindon in March 2004.

Conclusion

High-precision machining of electroceramics presents great challenges as the demand increases for fabrication of geometrically perfect sensors and actuators at miniature dimensions. The future of such devices depends on the achievement of efficient machining processes which do not compromise material properties or performance. This paper has presented aspects of the current status of precision dicing and grinding, with particular reference to recent developments in specialized equipment and in the understanding of machining at a micro-structural level. The collaboration between industry and academia has been especially fruitful in providing a synergy between differing areas of expertise. Further studies are encouraged to complement and expand existing work, and to accelerate progress in the field.

References

1. R.J. Dickinson, E.L. Nix, S.C. Davies, K.M. Morel, *Piezoelectric Transducer Arrays for Intravascular Ultrasound*, Proceedings of International Ferroelectrics Symposium, April 2001, Sheffield UK, I.M. Reaney & D.C. Sinclair (eds), Maney Publishing, London, pp. 101-112.

2. T. Bove, W. Wolny, E. Ringgaard, A. Pedersen, *New piezoceramic PZT-PNN material for medical diagnostics applications*, J. Eur. Ceram. Soc., 2001, **21**, 1469-1472.

3. A. Garg, T.C. Goel, *Mechanical and electrical properties of PZT ceramics (Zr:Ti = 0.40:0.60) related to Nd^{3+} addition*, Materials Science and Engineering, 1999, B**60**, 128-132.

4. P.-H. Xiang, X.-L. Dong, C.D. Feng, Y.L. Wang, *Mechanical and electrical properties of small amounts of In_2O_3 reinforced PZT ceramics*, Key Eng. Mater., 2003, **249**, 87-90.

5. P.-H. Xiang, X.-L. Dong, H. Chen, Z. Zhang, J.-K. Guo, *Mechanical and electrical properties of small amount of oxides reinforced PZT ceramics*, Ceram. Int., 2003, **29**, 499-503.

6. M. Stewart, W. Battrick, M. Cain, *Measuring Piezoelectric d_{33} Coefficients using the Direct Method*, Measurement Good Practice Guide No.44, June 2001, NPL Materials Centre, Teddington Middlesex, UK, TW11 0LW.

7. L. Lu, B.W. Chua, M.O. Lai, R.M. Johar, *Reduction in grain size of doped PZT ceramics for miniature sensors and actuators by ball milling technique*, Materials Science Forum, 2001, **360-362**, 615-622.

8. T. Karastamatis, D. Lupascu, S. Lucato, C. Lynch, *The effect of grain size on the R-curve behaviour of lead zirconate titanate (PZT)*, SPIE, 2001, **4333**, 38-40.

9. C.L. Davis, D.G. Morris, F.T. Calkins, *Characterization of fine grain piezoceramic stack actuators*, SPIE, 2001, **4333**, 441-451.

10. W. Weibull, *A Statistical Distribution Function of Wide Applicability*, J. Appl. Mech., 1951, **18**, 293.

11. H. Huang, P. Hing, *The relationship between the mechanical properties and microstructures of sintered PZT*, J. Mater. Proc. Tech., 1999, **89-90**, 538-543.

12. J. Yin, B. Jiang, W. Cao, *Determination of elastic, piezoelectric and dielectric properties of $Pb(Zn_{1/3}Nb_{2/3})O_3$ -$PbTiO_3$ single crystals*, Conference on Ultrasonic Transducer Engineering, San Diego, 1999, SPIE **3664**, 239-246.

13. S. Wan, C.S. Lynch, *Crack growth of PZN crystals under cyclic electric field*, SPIE, 2001, **4333**, 33-37.

14. S.W. Freiman, L. Chuck, J.J. Mecholsky, D.L. Shelleman, L.J. Storz, *Fracture Mechanisms in Lead Zirconate Titanate Ceramics*, Fracture Mechanics of Ceramics, 1986, **8**, 175-185.

15. T.-Y. Zhang, R. Fu, M. Zhao, P. Tong, *Overview of fracture of piezoelectric ceramics*, Key Engineering Materials, 2000, **183-187**, 695-706.

16. T.-Y. Zhang, *Studies of fracture of piezoelectric ceramics at HKUST*, Key Engineering Materials, 2000, **183-187**, 773-778.

17. H.G. Beom, S.N. Atluri, *Effect of electric fields on fracture behaviour of ferroelectric ceramics*, J. Mech. Phys. Solids, 2003, **51**, 1107-1125.

18. H. Jelitto, H. Keβler, G.A. Schneider, H. Balke, *Fracture behaviour of poled piezoelectric PZT under mechanical & electrical loads,* J. Eur. Ceram. Soc., 2005, **25**, 749-757.

19. Y. Shindo, M. Yoshida, F. Narita, K. Horiguchi, *Electroelastic field concentrations ahead of electrodes in multilayer piezoelectric actuators: experiment and finite element simulation*, J. Mech. Phys. Solids, 2004, **52**, 1109-1124.

20. A.A. Griffith, *The Phenomena of Rupture and Flow in Solids*, Phil. Trans. R. Soc., A, 1920, **221**, 163-198.

21. S.L. dos Santos e Lucato, H.-A. Bahr, V.-B. Pham, D.C. Lupascu, H. Balke, J. Rödel, U. Bahr, *Electrically driven cracks in piezoelectric ceramics: experiments and fracture mechanics analysis*, J. Mech. Phys. Solids, 2002, **50**, 2333-2353.

22. B.-L Wang, Y.-W. Mai, *Strength evaluation of piezo-electric ceramics under transient thermal environments*, J. Am. Ceram. Soc., 2004, **87**, 929-936.

23. H. Kishimoto, *Cyclic fatigue in ceramics*, JSME Int. J., Series 1, 1991, **34**, 393-403.

24. P.M. Chaplya, G.P. Carman, *Electrical fatigue degradation for dissimilar poled regions in PZT-5H*, Am. Soc. Mech. Engineers, Aerospace Division, 1999, **59**, 105-110.

25. D. Fang, B. Liu, C.T. Sun, *Fatigue crack growth in ferroelectric ceramics driven by alternating electric fields*, J. Am. Ceram. Soc., 2004, **87**, 840-846.

26. I. Arias, S. Serebrinsky, M. Ortiz, *A cohesive model of fatigue of ferroelectric materials under electro-mechanical cyclic loading*, SPIE Smart Struct. Mater., 2004, **5387**, 371-378.

27. B. Zickgraf, G.A. Schneider, F. Aldinger, *Fatigue behaviour of multilayer piezoelectric actuators*, IEEE Int. Symp. on Applications of Ferroelectrics, 1994, 325-328.

28. S.H. Ferguson, H.W. King, D.F. Waechter, R. Blacow, S.E. Prasad, *Crack growth in lead magnesium niobate-lead titanate ceramics by cyclic electric fields*, SPIE Smart Struct. Mater., 2004, **5387**, 513-518.

29. J. Rödel, W.S. Kreher, *Modeling cyclic fatigue phenomena of polycrystalline ferroelectric ceramics*, SPIE Smart Struct. Mater., 2001, **4333**, 261-270.

30. L.Z. Jiang, C.T. Sun, *Analysis of indentation cracking in piezoelectric ceramics*, Int. J. Solids Structures, 2001, **38**, 1903-1918.

31. T. Karastamatis, C.S. Lynch, *A method for measuring the mode-I fracture toughness in lead zirconate titanate (PZT)*, SPIE Smart Struct. Mater., 2000, **3992**, 156-164.

32. B.L. Wang, Y.G. Sun, *Intensity factors for some common piezoelectric fracture mechanics specimens with conducting cracks or electrodes*, Int. J. Eng. Sci., 2004, **42**, 1129-1153.

33. C.M. Landis, *On the fracture toughness of ferroelastic materials*, J. Mech. Phys. Solids, 2003, **51**, 1347-1369.

34. M. Alguero, C. Alemany, L. Pardo, A.A. Gonzalez, *Method for obtaining the full set of linear electric, mechanical and electromechanical coefficients and all related losses of a piezoelectric ceramic*, J. Am. Ceram. Soc., 2004, **87**, 209-215.

35. R. Jourdain et al, *Precision Multi-point Grinding of Commercial PZT Wafers for Piezoelectric Micro-actuators*, Proc. 4th Int. Conf. of European Society for Precision Engineering and Nanotechnology, May 31st – June 2nd 2004, Glasgow, Scotland, euspen HQ, Cranfield, UK, 137-138.

36. J. Corbett, D.J. Stephenson, *The Control of Surface Integrity by Precision Machining and Machine Design*, Proc. 1st Int. Conf. on Precision Machining, 2001, Usti nad Labem, Czech Republic, 31-43.

37. D.J. Stephenson, *Surface Integrity Control During the Precision Machining of Brittle Materials*, 6th Int. Symp. on Hybridized Materials with Super-Functions, 9-11 Dec 2004, Guanajuato, Mexico.

38. P.A. Beltrao, *Analysis of the Potential for Ductile Mode Machining of Ferroelectric Ceramic Materials*, PhD Thesis, Cranfield University, 1998.

39. H. Ohmori, *Electrolytic In-Process Dressing Grinding Technique for Ultra Precision Mirror Surface Machining*, JSPE, 1992, **26**(4).

40. H. Ohmori, T. Nakagawa, *Utilization of non-linear conditions in precision grinding with ELID for fabrication of hard material components*, Annals of the CIRP, 1997, **46**(1), 261-264.

41. R. Buttner, *Electrolytic Dressing of Diamond Wheels for use in Steel Grinding*, IDR, Nov. 1969, 205-208.

42. K. Lindsey, *Tetraform Grinding*, Commercial applications of precision manufacturing at the sub-micron level, SPIE, 1991, **1573**, 129-135.